Prediction of Ultrasonic Welding Parameters for Polymer Joining

Using first-principles equations to predict appropriate parameters for ultrasonic welding of polymers

BY M. MARCUS AND E. SANCAKTAR

Abstract

Welding of polymers is a useful assembly process that eliminates the need for adhesives or mechanical fasteners, saving consumable costs. One of the most common polymer welding processes is ultrasonic welding. Effective welding requires that the molten polymer chains at the joint surface diffuse across the joint and become entangled with polymer chains in the parts to be welded. This intermolecular diffusion and chain entanglement are the fundamental characteristics of welding. Using fundamental theories of heat generation and melt flow, optimal weld parameters can be calculated to ensure that diffusion across the weld joint occurs during ultrasonic welding.

Keywords

- Polymer Welding
- Ultrasonic Welding
- Intermolecular Diffusion
- Welding Parameters

Introduction

Ultrasonic welding is widely used in the plastics industry. In this process, mechanical deformations generate heating in the polymer via viscoelastic losses. Figure 1 provides an overview of the mechanical vibration system and the key interfaces.

A defined set of plastic welding experiments was completed using predicted parameters based on equations for weld speed, weld time, and weld force that were derived here for the first time from established theory. During experimentation, the dependent variable measured was tensile strength. Additionally, the parts were cross-sectioned to examine for signs of intermolecular diffusion. Controlled variables included ambient temperature, alignment, leveling, and cleanliness of the joint surface.

Independent variables included:

- Part geometry
  - Distance from horn contact surface to joint, joint size, and type
- Key material properties
  - Phase transition temperatures: melting or glass transition
  - Moduli: elastic, loss, storage
  - Melt viscosity, density, tensile strength
- Process settings
  - Duration of vibration exposure
  - Force or velocity of collapse
  - Vibration amplitude
  - Ultrasonic frequency

Derived Equations

Three equations were derived for the first time here from an established theory to be applied to ultrasonic welding process parameters. The equations provide a baseline for setting the weld speed, force, and time. Finding equations that depend on easily found and commonly measured polymer properties was an important consideration for this work. The equations are summarized here, and the derivations are in the appendix.

Melt flow index (MFI) is a standard measure of the viscosity of a polymer in terms of the volume of material that flows through a small aperture within 10 min under a set temperature and load. In 1983, Shenoy et al. showed that the MFI value for a different temperature and load could be approximated using the power law model from the original measurement. These equations are provided in the appendix. By approximating the MFI at the expected welding temperature and force, this polymer property can be used to predict an ideal weld speed using the derived Equation 1:

$$\text{Weld Speed} = R = \frac{\text{MFI}}{1200\rho x \tan\left(\frac{\theta}{2}\right) L} \quad (1)$$

https://doi.org/10.29391/2024.103.027

where R is the rate of flow normal to the faying surface in cm/s (which can be used as the weld speed), MFI is the melt flow index in g/10 min at the weld force and the material's critical flow temperature, ρ is the density in g/cm^3, x is the collapse distance, θ is the angle of the energy director, and L is the overall length of the energy director.

The properties needed to predict an ideal welding time are the polymer's heat capacity, density, loss modulus, and critical flow temperature. The critical flow temperature is the temperature at which a polymer begins to act more like a liquid than a solid (Ref. 1). For semi-crystalline polymers, this is simply the melting temperature. The critical flow temperature for amorphous polymers is the glass transition temperature, T_g +

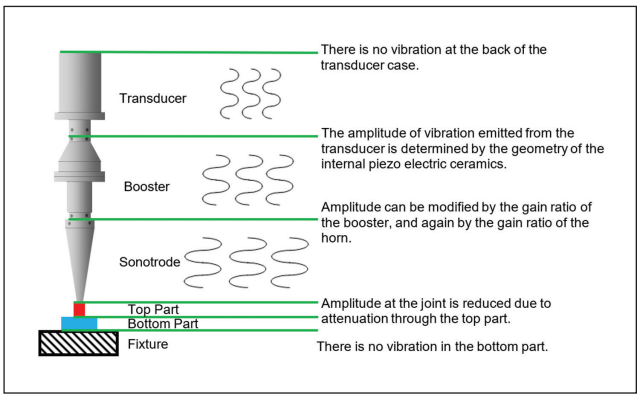

Fig. 1 — Diagram and description of amplitude at each interface present in the ultrasonic system's mechanical vibration portion.

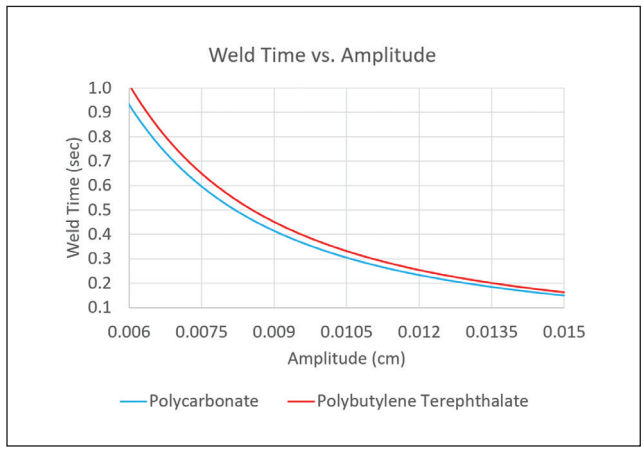

Fig. 2 — Calculated weld time vs. amplitude.

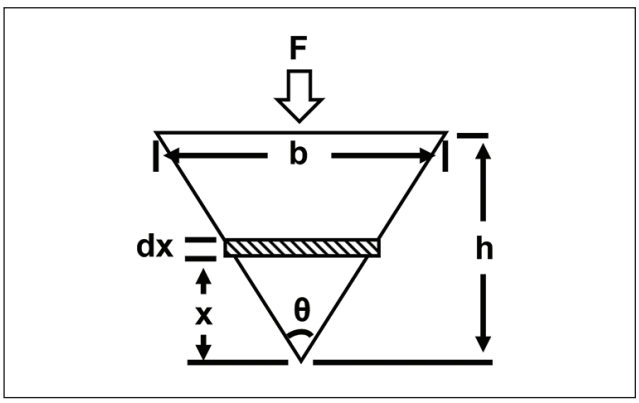

Fig. 3 — Diagram of energy director geometry and force applied.

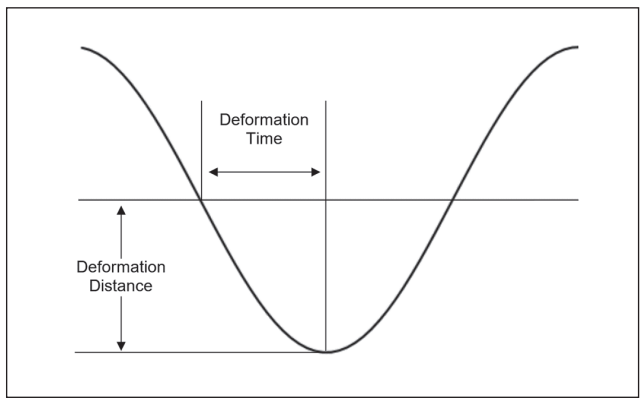

Fig. 4 — Diagram of polymer deformation due to ultrasonic vibration.

Table 1 — Inputs for Max Force Equation and the Calculated Results

	Polycarbonate	Polybutylene Terephthalate
ED Base (mm)	0.43	0.43
ED Height (mm)	0.38	0.38
ED Length (mm)	90.2	90.2
Young's Modulus (MPa)	2390	2650
Max Allowable Deformation (mm)	0.013	0.013
Max Compressive Force (N)	738.1	818.9

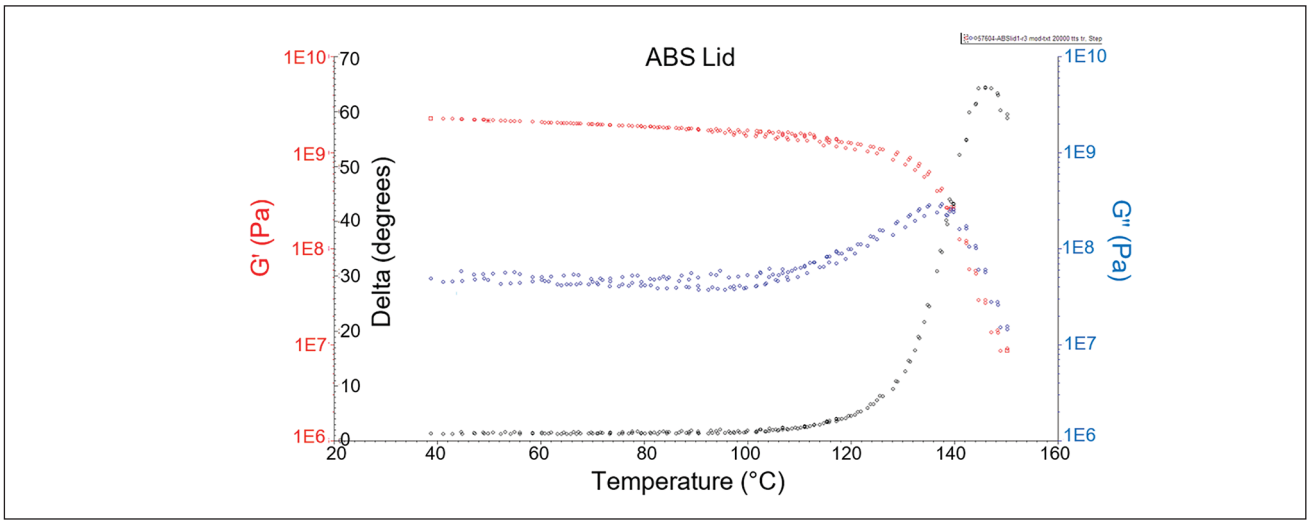

Fig. 5 — TTS curves for ABS at 20 kHz.

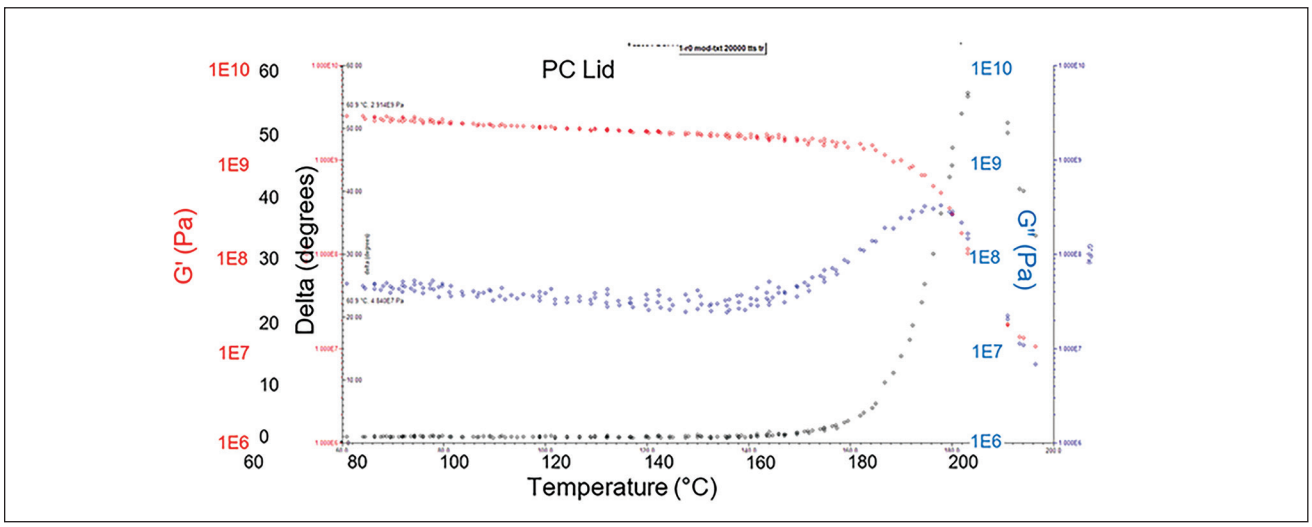

Fig. 6 — TTS curves for PC at 20 kHz.

100°C. Calculating the energy needed to reach the critical flow temperature and the expected heating rate during ultrasonic welding at the selected frequency and amplitude for the geometry of the parts can predict the weld time using Equation 2.

$$\text{Weld Time} = t_w = \frac{2\rho C_p T_F}{\omega E'' \left(\frac{\delta x}{dx}\right)^2} \quad (2)$$

where t_w is the weld time, ρ is the density, C_p is the heat capacity, T_F is the critical flow temperature, ω is the frequency, E" is the loss modulus, δx is the deformation, and dx is the energy director height.

Using this equation, the estimated weld times for different amplitudes show a reasonable weld time prediction, as shown in Fig. 2. The relationship of increasing amplitude to decreasing weld time and the magnitude of values for each align well with published ultrasonic welding parameters and is reasonable. In the *Handbook of Plastics Joining*, ultrasonic weld times reported for Polycarbonate (PC) range from 0.25–0.35 sec-

Table 2 — Frequencies for DMA Measurement

DMA Frequencies (Hz)
100
50
20
10
5
2
1

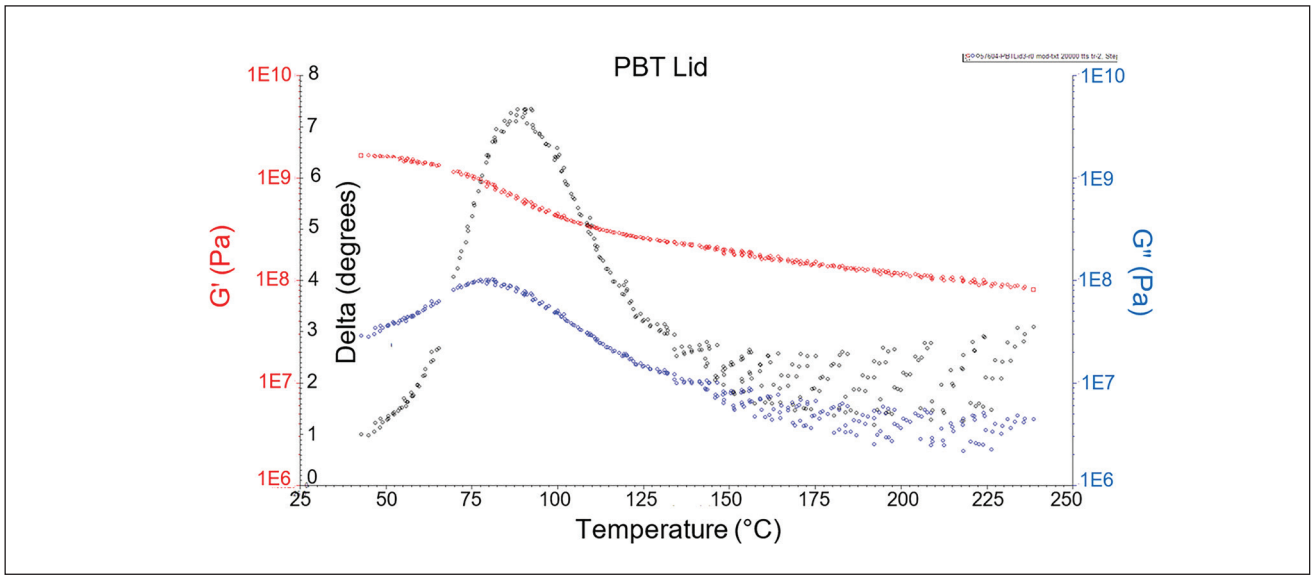

Fig. 7 — TTS curves for PBT at 20 kHz.

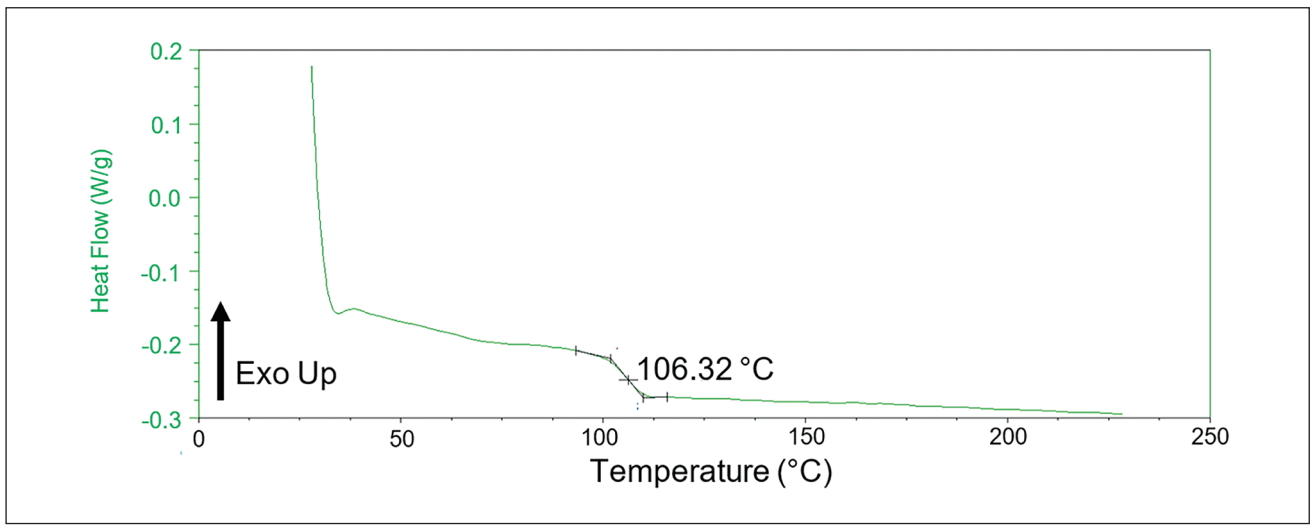

Fig. 8 — DSC curve for ABS.

Table 3 — Moduli at 20 kHz

Material	Type	E' (MPa)	E" (MPa)
ABS	Cups	1807	52.8
ABS	Lids	2274	48.5
PBT	Cups	1680	29.2
PBT	Lids	1661	28.6
PC	Cups	2247	46.4
PC	Lids	2914	48.4

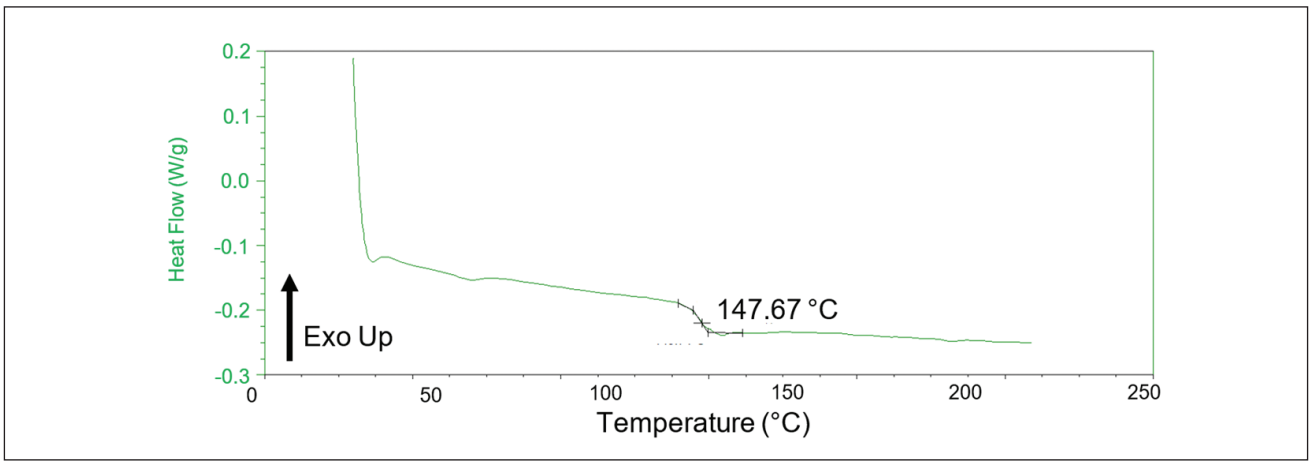

Fig. 9 — DSC curve for PC.

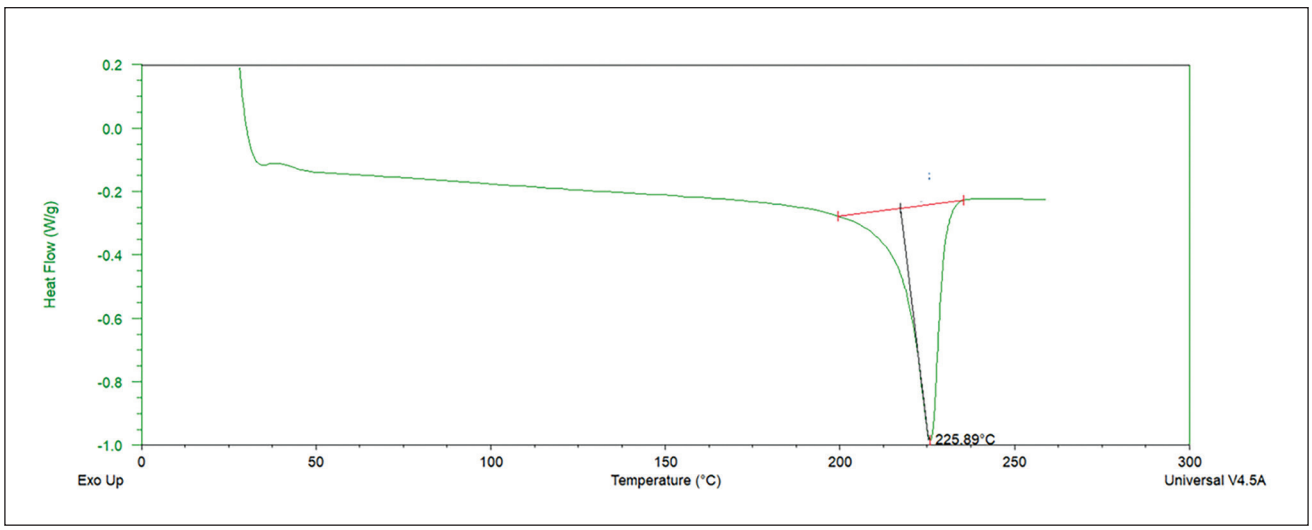

Fig. 10 — DSC curve for PBT.

onds, and weld times reported for Polybutylene Terephthalate (PBT) range from 0.5–1.0 seconds (Ref. 2).

The primary assumption made to derive an equation to predict weld force is that it is desirable to use a welding force that will not excessively deform the polymer at room temperature. From this assumption, Equation 3 was derived using the modulus of the polymer and the basic geometry of the parts to be welded. A diagram of the energy director detailing the important geometry for this calculation is shown in Fig. 3.

$$\text{Weld Force} = F = \frac{EbL\delta x}{hln\,(h)} \qquad (3)$$

where F is the force at which the deformation (δx) occurs, E is the elastic modulus, b is the width of the base of the energy director, L is the overall length of the energy director, and h is the height of the energy director.

Table 1 shows the force that would result in 0.013 mm or less plastic deformation using Equation 3. Using greater force will result in more initial flattening of the energy director and will thus increase the energy needed to initiate melting. This table shows values for a hypothetical part with a 60-degree energy director for PC and PBT.

Experimental observations demonstrated that, as a general trend, increasing force, when not sufficient to cause deformation or deflection in the part wall, improves weld strength. One possible reason is that this is is due to a decrease in the hammering coefficient, an effect proposed by Palardy et al. (Ref. 3).

Subsequently, it is proposed that the minimum force required to increase the hammering coefficient to approximately one can be calculated, thus negating its effect. Enough force should be applied to ensure that the deformation response of the polymer can be achieved within the time that the compression is applied. The amount of deformation is simply the 0-peak amplitude of the horn. The time scale for this deformation to occur is equivalent to one-quarter of the period of the ultrasonic wave. The diagram shown in Fig. 4 illustrates the deformation cycle.

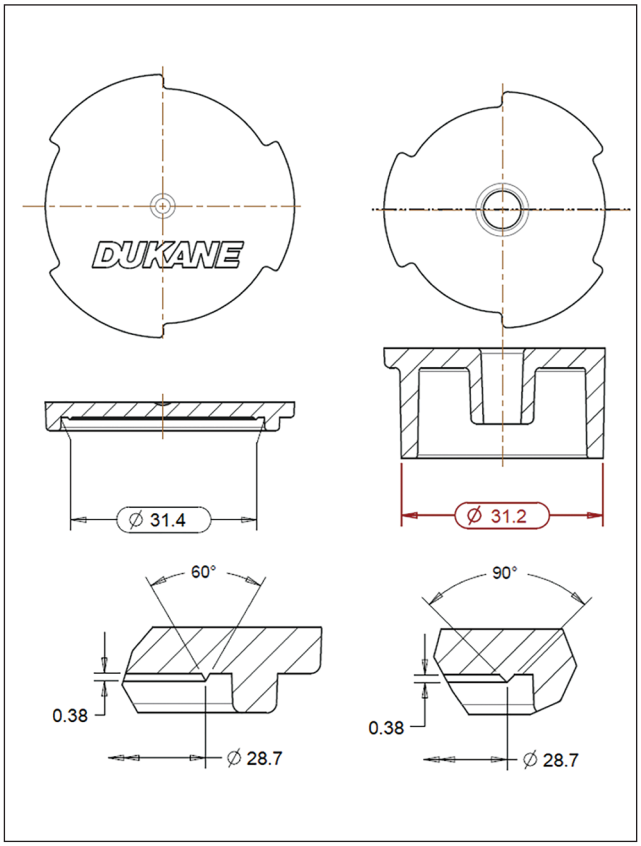

Fig. 11 — ISTeP part design.

Experimentation

Materials

Two amorphous and one semi-crystalline polymers were used:

- Amorphous
  - ABS: SABIC Cycolac MG47
  - PC: SABIC Lexan 124R-112
- Semi-crystalline
  - PBT: SABIC Valox 325

The softer amorphous polymer (ABS) was used with a 90-degree energy director. The harder amorphous polymer (PC) and the semi-crystalline material (PBT) were molded with a 60-degree energy director. Each material was chosen to have no fillers, additives, or colorants. Additionally, material grades were selected for which material data was readily available in the MoldEx simulation software.

The material properties needed for plastic ultrasonic welding and joint strength prediction model include:

- Loss/Elastic Modulus
- Heat Capacity
- Glass Transition Temperature
- Melting Temperature
- Heat of Fusion
- Density
- Melt Flow Index or Viscosity

All the properties were directly measured except the melt flow index, which was taken from the manufacturer's data

Table 4 — Heat Capacity Values

Material	Type	Sample	Cp (J/g°C)	Average
ABS	Cup	1	1.3442	1.345
ABS	Cup	2	1.3621	
ABS	Lid	1	1.3411	
ABS	Lid	2	1.3326	
PBT	Cup	1	1.3165	1.336
PBT	Cup	2	1.3434	
PBT	Lid	1	1.3327	
PBT	Lid	2	1.3517	
PC	Cup	1	1.3383	1.336
PC	Cup	2	1.3636	
PC	Lid	1	1.3267	
PC	Lid	2	1.3158	

Table 5 — Melt Flow Indices

Material	MFI (g/10 min)	Load (kg)	Temperature (°C)
ABS	5.6	3.8	230
PC	17.5	1.2	300
PBT	50	5.0	265

Table 6 — Density Measurements

	Width 1 and 2 (cm)		Length 1 and 2 (cm)		Height 1 and 2 (cm)		Volume (cm^3)	Weight (g)	Density (g/cm^3)
PC Cup 1	7.95	8.00	8.95	8.90	2.93	2.94	0.209	0.2434	1.165
PC Cup 2	7.54	7.48	7.91	7.86	2.96	2.94	0.175	0.2110	1.208
PC Lid 1	6.01	5.94	9.74	9.72	2.39	2.39	0.139	0.1593	1.146
PC Lid 2	5.68	5.92	9.89	10.03	2.37	2.37	0.137	0.1544	1.128
PBT Cup 1	5.63	5.30	7.52	7.54	2.88	2.89	0.119	0.1523	1.283
PBT Cup 2	5.64	5.65	7.55	7.60	2.89	2.90	0.124	0.1571	1.269
PBT Lid 1	4.92	4.93	9.54	9.50	2.28	2.27	0.107	0.1376	1.290
PBT Lid 2	4.50	4.47	9.47	9.56	2.28	2.28	0.097	0.1276	1.311
ABS Cup 1	6.11	6.13	10.17	10.16	3.04	3.08	0.190	0.1919	1.008
ABS Cup 2	5.83	5.50	10.21	10.18	3.05	3.08	0.177	0.181	1.022
ABS Lid 1	10.07	10.05	11.73	11.81	2.30	2.31	0.273	0.284	1.041
ABS Lid 2	9.35	9.30	11.91	11.89	2.31	2.31	0.256	0.2647	1.033

Table 7 — Amplitude Measurement Results, 20-kHz Horn

Input Amplitude (%)	Measured Amplitude (μm p-p)							
	Linear Vibrometer				Displacement Gauge			
	A	B	C	D	A	B	C	D
20	16	16	16	16	4	6	5	4
30	24	24	24	24	12	14	14	12
40	31	31	31	32	20	20	20	18
50	39	39	39	39	28	26	28	24
60	46	46	46	46	34	34	34	30
70	54	53	54	54	42	40	40	40
80	61	61	61	61	48	46	46	46
90	71	71	72	71	54	52	52	52
100	78	79	78	79	62	62	60	62

sheet. The moduli were measured via dynamic mechanical analysis (DMA). The heat capacity and transition temperatures were measured using dynamic scanning calorimetry. The density was indirectly determined through volume and weight measurements.

The loss modulus is dependent on temperature and frequency. Tests were performed at different temperatures to find the loss modulus values at different ultrasonic frequencies. Loss modulus measurements were made at low frequencies over a temperature range. Time-temperature superposition (TTS) was used to calculate loss modulus for higher frequencies. The DMA was set to measure the samples in 10°C increments, starting at 30°C, until a maximum temperature was reached that was selected for each material. For ABS, the max was 150°C. For PC and PBT, the max was 190°C. The frequency sweep at each test temperature is shown in Table 2.

A single cantilever setup was used. Small sections of the iSTeP molded bases and lids were machined to the needed 1- × 12- × 35-mm size. Parts were machined to be tested for each material, equally divided between the bases and lids.

After collecting the data, TTS was calculated using the Williams–Landel–Ferry (WLF) equation (Ref. 4). TTS is ideally applied for amorphous polymers at temperatures below their T_g. Further, it is best to make measurements at low temperatures to find moduli at high frequencies. However, the available DMA did not have cooling capability, so the high-frequency moduli were predicted for a temperature greater than room temperature. This was considered an acceptable approximation since the material is heated during welding and does not remain at room temperature for long. TTS was also applied to the semi-crystalline materials, although the calculations were expected to produce less accurate results.

The data provided a relatively clean fit for all four materials at high frequencies. Figures 5–7 show the TTS curves for the lid components for each of ABS, PC, and PBT materials at 20 kHz. The data at each frequency sweep for each temperature have been superimposed and shifted to represent the material properties at 20 kHz.

The DMA data was also used to determine the elastic moduli of these three materials. The moduli for the cups and lids for each material, extrapolated for 20 kHz at room temperature, are shown in Table 3. Although the same material was used for the cups and lids, each had different injection molding process settings. Due to that and the difference in geometry, slight differences in the material properties will occur.

A dynamic scanning calorimeter (DSC) was used to measure the heat capacity, heat of fusion, and transition temperatures; Figs. 8–10 show one DSC curve for each of the materials.

The DSC curve shows heat flow during heating, and the thermal behavior of the material is used to measure transition temperatures and heat of fusion (if applicable). Two cup samples and two lid samples were measured for each material. A reference measurement using a sapphire sample was taken to find the heat capacity.

Equation 4 was used to calculate the heat capacity for each material:

$$C_{p_{test}} = C_{p_{ref}} \left(\frac{X_{test}}{X_{ref}}\right)\left(\frac{W_{ref}}{W_{test}}\right) \quad (4)$$

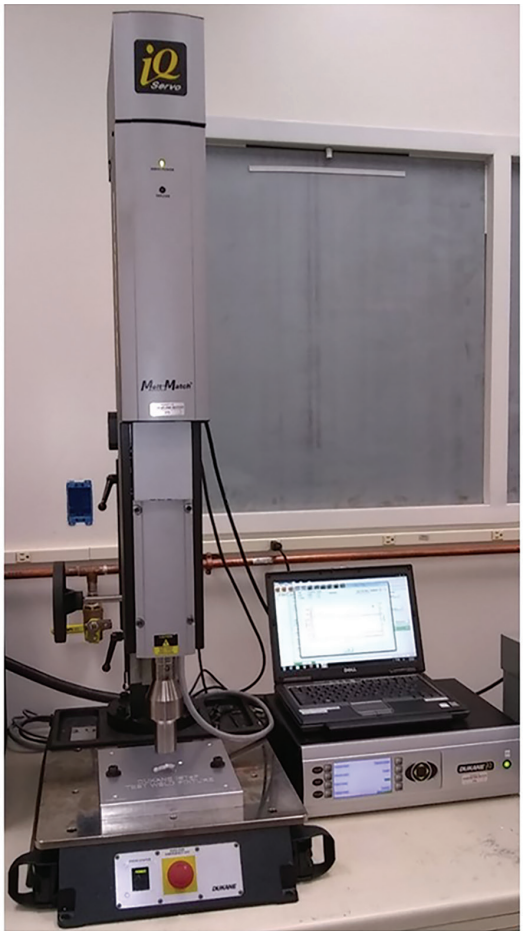

Fig. 12 — Servo-driven ultrasonic welding machine.

where C_p is the heat capacity, X is the offset from the nominal from the DSC run, and W is the weight of the sample.

Table 4 shows the heat capacity values for each material as found via the DSC measurements and calculated using Equation 16.

Each material's melt flow index values were sourced from matweb.com and are shown in Table 5.

The material density was measured by taking three rectangular bar samples of each material and measuring the minimum and maximum width, thickness, and length of each. Subsequently, each piece was weighed using a precision scale. The measurements of the samples and the calculated density for each material are shown in Table 6.

ISTeP™ Parts were used for the experimental trials, which were developed to allow for five different types of joint design and several different welding methods. Figure 11 shows the design of these parts with the energy director designs used for this work.

Equipment and Tooling

A Dukane iQ Servo-Driven Ultrasonic Welder was used to weld the parts, as shown in Fig. 12.

A simple flat-face horn was used. The amplitude at the horn face was measured using a laser vibrometer and a mechanical displacement gauge at four locations on the horn face, as shown in Fig. 13. The measurements using both methods were consistent for each device but did not have good agreement with each other. These results are shown in Table 7.

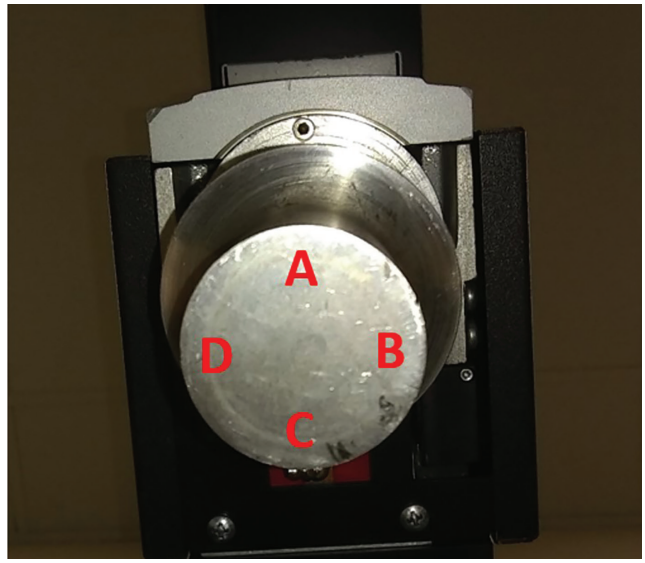

Fig. 13 — Amplitude measurement locations.

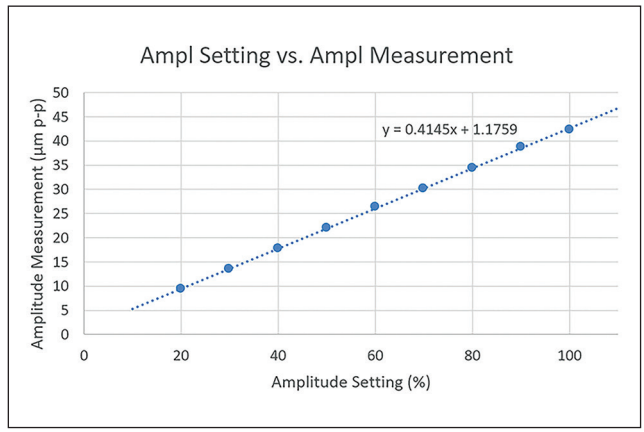

Fig. 14 — Measured amplitude vs. programmed amplitude percentage at 20 kHz, location A.

The results from the laser vibrometer measurements are expected to be more accurate and were used to calculate the weld settings. The measured amplitude provided a relationship between the programmable amplitude percentage and the resulting amplitude on the horn face, as shown in Fig. 14. The resulting linear equation can be used to convert the desired output amplitude into the amplitude percentage that can be programmed into the weld process controller.

A close-up of the flat face horn and fixture is shown in Fig. 15. The fixture provided a simple location of the parts. The fixture was precisely leveled using the set screws in each corner of the plate for adjustment.

Six assemblies were welded with each parameter set. Of these, five were tensile tested using an Instron tensile tester,

Table 8 — Approach to Define Weld Parameters			
	Weld Speed (mm/s)	Time to Melt (s)	Trigger Force (N)
Equation	6	10	15
Value	1.58	0.24	315.3

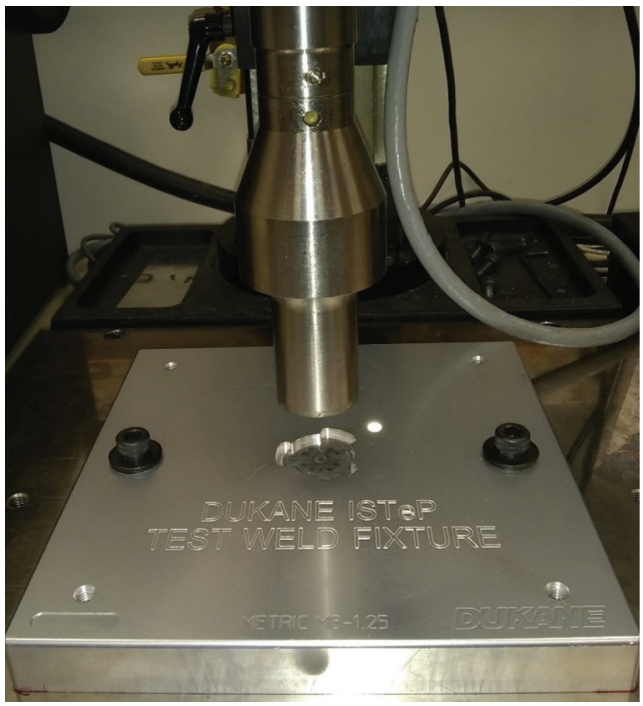

Fig. 15 — Horn and fixture.

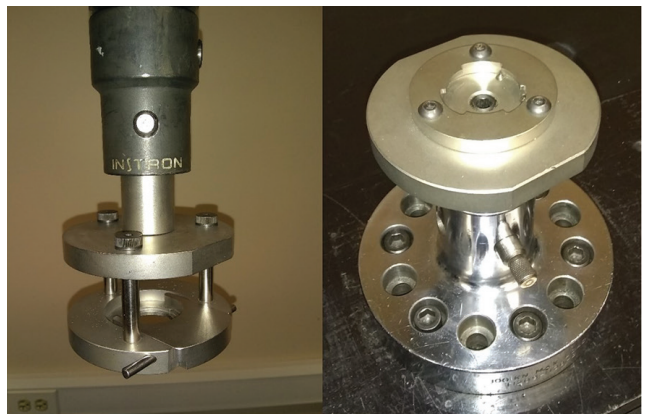

Fig. 16 — Tensile testing tooling: top (left); bottom (right).

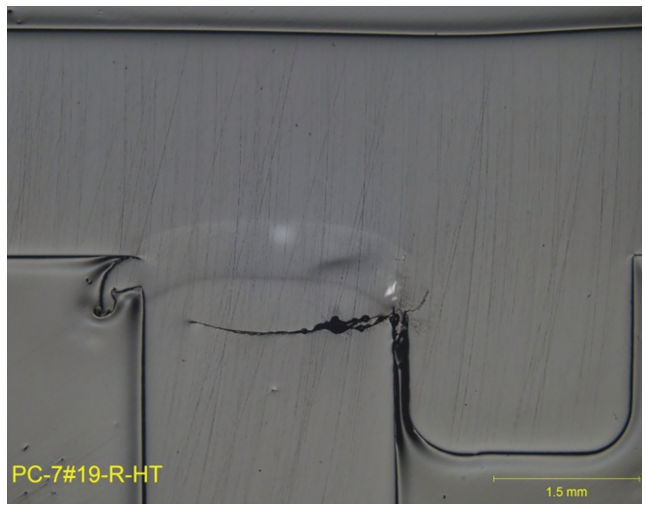

Fig. 17 — PC, 20 kHz, 0.44-mm collapse, 374-N trigger force, 0.035-mm amplitude.

and one was cross-sectioned. The tooling used for tensile testing is shown in Fig. 16.

The tensile tests were performed using a displacement rate of 50 mm/min, a preferred rate that enables comparison to base material data per ASTM D638, listed on matweb.com. The force was recorded in Newtons (N). Then, the weld width was measured using the cross-section results on two opposite sides of the weld. This measured width was used to calculate the average weld area, which was used to convert the strength results from force (N) to stress (MPa) to enable comparison with the base material strength data.

Process Parameter Calculations

The preliminary weld time, weld speed, and trigger force were calculated using the equations described in the appendix. The weld distance was adjusted based on the part geometry. The hold speed was set to the same value as the weld speed, and the hold distance was set to 1/10 of the weld distance.

Amplitude, force, and speed are co-dependent welding parameters. The ultrasonic heat generation was used to predict the initial heating rate. The total cycle time was determined by dividing the work needed by the heat generation rate using Equation 1. This gave an estimated welding time.

The plastic deformation that occurs under a static load at room temperature was calculated. This deformation, an adjustment to the distance through which the ultrasonic wave must travel, was then accounted for in the amplitude calculations. Equation 3 was used to set the trigger force so that the average displacement rate matched the average heating rate.

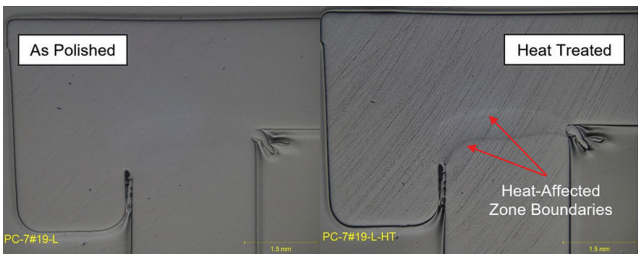

Fig. 18 — Cross section of PC weld showing good intermolecular diffusion.

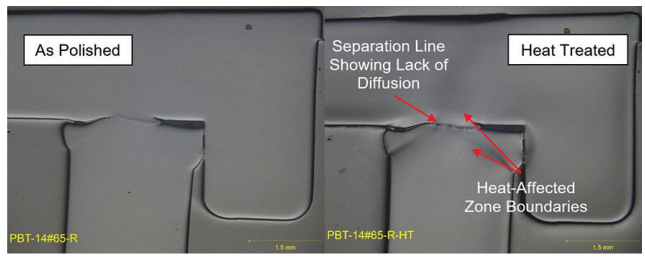

Fig. 19 — Cross section of PBT weld showing no intermolecular diffusion.

Table 9 — Properties, Dimensions, and Input Parameters Needed for Table 8

Material Properties		
E’ (MPa)	Storage Modulus	2274
E’’ (MPa)	Loss Modulus	48.5
E* (MPa)	Complex Modulus	2275
Cp (J/g°C)	Heat Capacity	0.85
T_F (°C)	Flow Temperature	230
ρ (g/cm^3)	Density	1.03
MFI (g/10 min)	Melt Flow Index at Flow Temperature	5.6
n	Power Law Index	0.25
Geometry		
θ (degrees)	Energy Director Angle	90
b (mm)	Energy Director Base Width	1.02
h (mm)	Energy Director Height	0.51
L (mm)	Energy Director Length	28.7
d (mm)	Distance from Horn Contact Surface to Energy Director Base	3
Input Process Parameters		
T_R (°C)	Room Temperature	25
c (mm)	Collapse Distance	0.38
A (mm)	Amplitude at Horn Contact Surface	0.03
f (Hz)	Frequency	20000

Table 8 shows how these equations were applied to find preliminary welding parameters when using the inputs, as shown in Table 9.

he final weld settings are shown in Table 10. These settings were all calculated using the approach shown in Table 8. The collapse distance was set shorter than the energy director height to ease the weld simulation and ensure purely tensile stress during testing. It was suspected that assuming an average heating speed of the semi-crystalline material was problematic, so two sets of weld parameters were used for the PBT parts, one with a constant speed and one using a segmented speed profile. The welder can perform ten discrete changes in the welding speed, so the time to heat each tenth of the energy director was calculated to find the appropriate welding speed for each segment, as shown in Table 11.

Table 10 — Experimental Welding Parameters

Material	Energy Director Angle (Degree)	Frequency (Hz)	Weld Collapse (mm)	Trigger Force (N)	Amplitude (mm)	Weld Speed (mm/s)	Hold Speed (mm/s)	Hold Collapse (mm)
ABS	90	20000	0.38	315	0.03	1.58	1.58	0.038
ABS	90	20000	0.25	315	0.03	1.58	1.58	0.025
ABS	90	20000	0.38	463	0.05	7.32	7.32	0.038
ABS	90	20000	0.38	391	0.04	3.75	3.75	0.038
ABS	90	30000	0.38	233	0.02	0.48	0.48	0.038
PC	60	20	0.38	374	0.035	0.52	0.52	0.038
PC	60	20	0.25	374	0.035	0.52	0.52	0.025
PC	60	20	0.38	496	0.04	0.78	0.78	0.038
PC	60	20	0.38	636	0.045	1.12	1.12	0.038
PC	60	30	0.38	435	0.035	0.65	0.65	0.038
PBT Constant Speed	60	20	0.38	1232	0.03	1.1	0.11	0.038
	60	20	0.25	1232	0.03	1.1	0.11	0.025
	60	20	0.38	909	0.025	0.66	0.066	0.038
	60	20	0.38	632	0.02	0.36	0.036	0.038
	60	30	0.38	634	0.02	0.36	0.036	0.038
PBT Profiled Speed	60	20	0.38	1232	0.03	A*	0.11	0.038
	60	20	0.25	1232	0.03	B*	0.08	0.025
	60	20	0.38	909	0.025	C*	0.05	0.038
	60	20	0.38	632	0.02	D*	0.02	0.038
	60	30	0.38	634	0.02	E*	0.02	0.038

*See Table 11 for the speed settings.

All the materials showed a tensile strength much reduced from the bulk resin values. It should be noted that all the welds have a sharp corner near the edge of the melt, which will act as a stress concentration feature. This is very likely a contributing factor to the reduced joint strength. The cross-sectional analysis shows this very clearly. In one of the PC sections, shown in Fig. 17, it can be observed that a crack had already formed across the bulk material near the edge of the weld flash on the right side. This demonstrates that the geometric (stress concentration) effects of the weld melt geometry are critical to weld strength.

Table 12 shows the base material strength for each material and the percentage of that strength that was achieved for each weld in Group 1.

All amorphous materials were welded well using the calculated weld parameters. Both ABS and PC showed a homogenous weld zone when cross-sectioned and heat treated, which indicated intermolecular diffusion had occurred. However, the semi-crystalline material, PBT, did not show a homogenous weld zone. The approximation of an average heating rate that was used is likely far more applicable to amorphous polymers than semicrystalline. The PBT welds made using a speed profile instead of a constant speed did appear to have better welds, but there is still significant room for improvement.

When a polished cross-section of the joint is heat treated by applying hot air or infrared radiation to the surface, the polymer chains on the top surface, which have been mechanically smeared during polishing, experience thermal recovery, and a distinct line appears where there has been a change in the microstructure of the part (Ref. 5). When a weld has good intermolecular diffusion, such as shown in Fig. 18, the heat-affected zone's boundaries appear, but there is no boundary line through the middle of the weld. When there is no diffusion, as in Fig. 19, a distinct line of separation can be seen at the interface.

The PC welds showed signs of full intermolecular diffusion after welding, as shown in Fig. 20.

The PBT welds show signs of good welding, but some appear to have pulled apart in the weld zone during cooling. The most evident example of this is shown in Fig. 21.

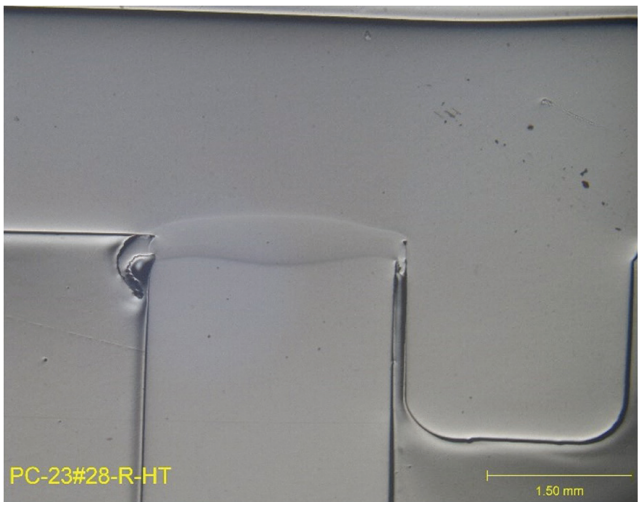

Fig. 20 — PC weld with intermolecular diffusion.

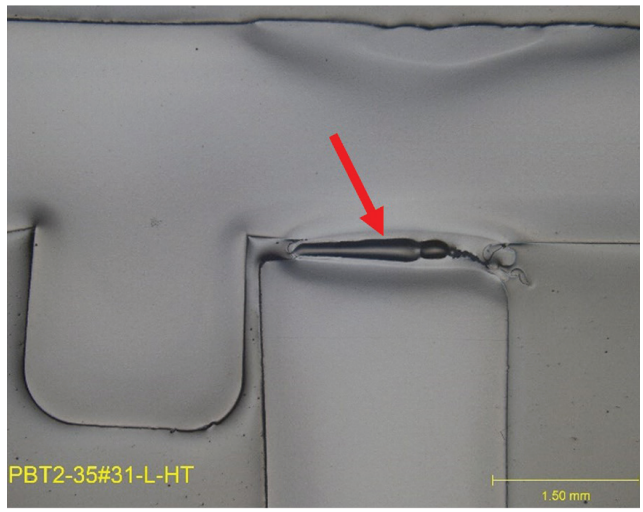

Fig. 21 — PBT, profiled speed, 20 kHz, 0.38-mm collapse, 634-N trigger force, 0.02-mm amplitude.

Table 11 — PBT Profiled Speed Settings (mm/s)

Speed Profile	Step 1	Step 2	Step 3	Step 4	Step 5	Step 6	Step 7	Step 8	Step 9	Step 10
A	0.4	0.5	0.7	0.9	1.0	1.0	1.1	1.5	2.6	11.3
B	0.4	0.5	0.6	0.7	0.8	1.0	1.0	1.0	1.0	1.1
C	0.2	0.3	0.4	0.5	0.4	0.4	0.4	0.6	1.0	3.6
D	0.12	0.15	0.19	0.16	0.14	0.14	0.15	0.19	0.31	1.03
E	0.15	0.19	0.23	0.24	0.21	0.21	0.22	0.28	0.47	1.56

Conclusions

As one of the most widely used polymer welding processes, it is important to grow our understanding of ultrasonic welding. This work provides a method to calculate weld process parameters, thus reducing process development time and the number of trials needed to achieve good results. An approach to calculating key process variables and the experimental results of applying these methods has been shown to be effective here. This approach applies to amorphous polymers using simple arithmetic and common material properties. An important next step is to expand this approach to semi-crystalline polymers, possibly with computer modeling approaches.

The formulae validated in this paper are:

$$\text{Weld Speed} = R = \frac{MFI}{1200\rho x \tan\left(\frac{\theta}{2}\right) L} \quad (1)$$

where R is the rate of flow normal to the faying surface in cm/s (which can be used as the weld speed), MFI is the melt

Table 12 — Strength of Welds vs. Bulk

Material	Frequency (kHz)	Collapse (mm)	Trigger Force (N)	Amplitude (mm)	Bulk Strength (MPa)	Weld Strength (MPa)	Weld Strength (%)
ABS	20	0.38	315	0.03	35	6.0	17.1%
	20	0.25	315	0.03		11.3	32.3%
	20	0.38	394	0.05		1.3	3.6%
	20	0.38	233	0.04		6.7	19.3%
	30	0.38	463	0.02		19.9	56.9%
PC	20	0.38	374	0.035	68	10.9	16.1%
	20	0.25	374	0.035		10.0	14.7%
	20	0.38	496	0.04		10.5	15.4%
	20	0.38	636	0.045		7.5	11.1%
	30	0.38	435	0.035		24.7	36.3%
PBT Constant Speed	20	0.38	1232	0.03	51	4.6	9.0%
	20	0.25	1232	0.03		1.8	3.6%
	20	0.38	909	0.025		3.7	7.3%
	20	0.38	632	0.02		2.4	4.6%
	30	0.38	634	0.02		10.6	20.9%
PBT Profiled Speed	20	0.38	1232	0.03		3.9	7.7%
	20	0.25	1232	0.03		2.1	4.2%
	20	0.38	909	0.025		6.8	13.4%
	20	0.38	632	0.02		6.2	12.2%
	30	0.38	634	0.02		5.1	10.0%

flow index in g/10min at the weld force and the material's critical flow temperature, ρ is the density in g/cm^3, x is the collapse distance, θ is the angle of the energy director, and L is the overall length of the energy director.

$$\text{Weld Time} = t_w = \frac{2\rho C_p T_F}{\omega E'' \left(\frac{\delta x}{dx}\right)^2} \quad (2)$$

where t_w is the weld time, ρ is the density, C_p is the heat capacity, T_F is the critical flow temperature, ω is the frequency, E'' is the loss modulus, δx is the deformation, and dx is the energy director height.

$$\text{Weld Force} = F = \frac{EbL\delta x}{h\ln(h)} \quad (3)$$

where F is the force at which the deformation (δx) occurs, E is the elastic modulus, b is the width of the base of the energy director, L is the overall length of the energy director, and h is the height of the energy director.

Acknowledgments

The researchers would like to thank Matt Nitsch for his excellent technician support.

Appendix

The derivations of the equations used in this work are described here.

Weld Speed

As the ultrasonic wave passes through a polymer, the viscoelastic properties of polymers promote heating at the joint. Similar to the attenuation and phase shift, equations to model the heat generation rate per unit volume, *Q*, for ultrasonic welding of plastic have been proposed in a few different variations. The most common form is Equation 5 (Refs. 6–9):

$$Q = \frac{1}{2}\omega E'' \varepsilon^2 \quad (5)$$

where ω is the ultrasonic frequency in radians, E'' is the material's loss modulus, and ε is the strain amplitude.

Essentially, this equation accounts for the energy lost due to the poor transmission of vibrations through the viscous portion of the polymer at the joint. The ultrasonic frequency and amplitude at the joint relate to the energy available for heating. The loss modulus is the material property that describes how mechanical actions are attenuated through the polymer. Referring to the Kelvin-Voight model, this can be thought of as the dashpot resistance to movement (Ref. 10). However, because energy does not simply cease to exist due to the law of conservation of energy, mechanical motions that are not translated become heat.

It should be noted that this method has shown a good correlation to experimental results (Refs. 11–14).

Empirical evidence shows that the molten material is displaced incrementally during ultrasonic welding. In other words, a small volume of melt is generated. This is pushed out of the way, then the solid part of the energy director contacts the mating surface, and a small new volume of melt is generated. This process is repeated until the end of the weld. Thus, the time needed to displace the generated melt layer should be considered when predicting weld parameters.

This displacement rate can be compared to the time required to heat the polymer to adjust important weld settings like the applied force and welding speed. Ideally, the melting and displacement rates would be equivalent to ensure no polymer degradation or lack of fusion in the weld.

To estimate the time for the energy director to displace, the MFI of the polymer can be used to estimate the flow speed. While viscosity data is infrequently measured and provided for commercial polymers, the melt flow index is widely available. Additionally, the melt flow index for an unknown pressure and temperature can be extrapolated from known data (Refs. 15, 16).

When the dimensions of the melt flow indexer are consistent, the MFI values can be calculated for other loads and temperatures using the following equations, which have been derived based on the ASTM guidelines for the geometry that should be used in a melt flow indexer (Ref. 16):

$$\ln\left(\frac{MFI_2}{MFI_1}\right) = \frac{8.86\,(T_2 - T_s)}{101.6 + (T_2 - T_s)} - \frac{8.86\,(T_1 - T_s)}{101.6 + (T_1 - T_s)} \quad (6)$$

$$\left(\frac{MFI_2}{MFI_1}\right) = \left(\frac{L_2}{L}\right)^{\frac{1}{n}} \quad (7)$$

where MFI_1 is the melt flow index at T_1/L_1, MFI_2 is the melt flow index at T_2/L_2, T_s is the glass transition temperature +50°C, and n is the power law index.

For this work, the power law index has been approximated using published data for common polymers (Ref. 17). For Acrylonitrile Butadiene Styrene (ABS), a value of 0.25 was used. For Polycarbonate (PC), a value of 0.70 was used, and for Polybutylene terephthalate (PBT), a value of 0.60 was used.

Once a temperature has been predicted for the melt flow in the ultrasonic weld and the applied load has been determined, the MFI at these values can be extrapolated and can then be used to get an approximation of the rate of deformation of the energy director using Equation 8 (Ref. 18):

$$R = \frac{MFI}{600\rho wL} \quad (8)$$

where *R* is the rate of flow (mm/min), MFI is the melt flow index (g/10 min), ρ is the density (g/mm^3) of the plastic, w

is the width (mm) of the energy director, and L is the length (mm) of the energy director.

For a triangular geometry, the width of the energy director as a function of distance (x) from the tip of the triangle can be defined by:

$$w = 2x\tan\left(\frac{\theta}{2}\right) \tag{9}$$

Equations 8 and 9 can then be combined to obtain Equation 10 for approximate rate of flow versus collapse distance, x, which can be used for an ultrasonic welding process that uses a constant load, rather than a constant velocity, of displacement:

$$\text{Weld Speed} = R = \frac{MFI}{1200\rho x\tan\left(\frac{\theta}{2}\right)L} \tag{1}$$

where R is the rate of flow normal to the faying surface in cm/s, MFI is the melt flow index in g/10 min, ρ is the density in g/cm^3, x is the collapse distance, θ is the angle of the energy director, and L is the overall length of the energy director.

Weld Time

The heating equation can subsequently be used to determine the heating time required to melt the energy director in terms of energy dissipation per unit time per unit volume. To do this, it is assumed that all amplitude not lost by attenuation or phase shift provides the necessary deformation to heat the energy director.

A further assumption is made that the volume heats uniformly. In practice, plastic welding researchers know that this is not the case. The heating of the energy director proceeds from the tip towards the base, with each layer of melt being pushed out of the way to allow absorption of the vibrational energy in the newly exposed solid contact interface, followed by melting this subsequent section of the energy director. As the energy director shortens, so does the reference length, leading to a change in strain and heating rate. However, assuming a consistent heating rate still leads to a realistic prediction of weld time based on previous experiments.

We start with the basic heating equation to find the heating rate, ΔT:

$$\Delta T = \frac{Q/V}{\rho C_p} \tag{10}$$

where Q/V is the internal heat generation rate per volume, ρ is the density of the material, and Cp is the specific heat capacity of the polymer.

The time to reach the melting temperature, weld time, is:

$$t_w = \frac{T_F}{\Delta T} \tag{11}$$

where t_w is the weld time, T_F is the critical flow temperature, and ΔT is the heating rate.

The critical flow temperature is the temperature above which the polymer melt behavior changes from that of a viscoelastic solid to that of a liquid. At this point, the pressure applied during welding pushes the melt away from the joint.

To continue the calculation of ideal melt time, Equations 10 and 11 are combined:

$$t_w = \frac{\rho C_p T_F V}{Q} \tag{12}$$

By substituting in the equivalent of Q'/V from Equation 5, the equation becomes:

$$\text{Weld Time} = t_w = \frac{2\rho C_p T_F}{\omega E''\left(\frac{\delta x}{dx}\right)^2} \tag{2}$$

where ρ is the density, C_p is the specific heat capacity, T_F is the critical flow temperature, ω is the ultrasonic frequency in radians, E'' is the loss modulus, δx is the instantaneous deformation, and dx is the energy director height.

By inputting known material properties of PC and PBT, as well as the geometry of a known Industrial Standard Test Part (iSTeP), estimated weld times for different amplitudes (considered the instantaneous deformation) can be calculated (note: a known and easily obtained iSTeP is planned for the experimental validation of this model).

Force

Previous experimental research has shown that weld strength generally increases with increased force up to a maximum and then levels out or decreases (Ref. 19).

The reason for a maximum force before strength starts to degrade has been proposed to be due to two distinct factors. The most cited reason is that above the maximum force, the energy director of the part deforms and prevents good melt initiation due to a reduction in stress concentration. The other proposition is that excessive force can lead to highly oriented polymer chains that weaken the tensile strength. This work examines the energy director's deformation issue (Ref. 20).

The amount of force to be applied to the parts should not cause the plastic to deform prior to reaching the critical flow temperature. A mechanical deformation problem for the triangular energy director has been used to find an equation to define this limit.

This proposed approach to finding the maximum force that can be applied without causing deformation begins with the stress-strain relationship, $\sigma = E\varepsilon$, where σ is stress, E is the modulus, and ε is strain.

From this, the relationship between the strain, applied force, and modulus can be found:

$$\varepsilon = \frac{\delta x}{dx} = \frac{\sigma}{E} = \frac{F/a}{E} = \frac{F}{aE} \tag{13}$$

where δx is the deformation, F is the applied force, a is the area:

$$a = \frac{b}{h} xL \tag{14}$$

where b is the width of the energy director base, h is the height of the energy director, and L is the overall length of the energy director.

Rearranging and integrating over the cross-section:

$$\delta x = \frac{F}{E} \int_0^h \frac{1}{\frac{b}{h} xL} \tag{15}$$

Which resolves to:

$$\delta x = \frac{F}{E} \frac{h}{bL} \ln(h) \tag{16}$$

However, in this case, we want to solve for the force, so the equation can be rearranged:

$$\text{Weld Force} = F = \frac{EbL\delta x}{h \ln(h)} \tag{3}$$

where F is the force at which the deformation (δx) occurs, E is the elastic modulus, b is the width of the base of the energy director, L is the overall length of the energy director, and h is the height of the energy director.

While Equation 3 can provide a good guideline for maximum force to avoid over-compressing the energy director, a minimum force required also needs to be considered. There are two main considerations for the minimum force. First, there must be ample force to push the polymer melt out of the joint. Second, there must be adequate force to ensure that the ultrasonic vibrations are fully transferred to the polymer.

The provision of ample force to push the melt out of the joint is more difficult to calculate. Because the viscosity of the polymer melt is non-Newtonian, it varies with temperature and load. Therefore, to define a minimum force to establish a set point for the simulation, this study will focus on applying adequate force to ensure there is no loss of contact between the polymer and the horn during ultrasonic vibrations. The possibility for loss of contact has been noted previously by researchers, who have accounted for this effect by introducing a "hammering coefficient" to the heating equation to account for the loss in amplitude due to insufficient coupling (Ref. 3).

Prior analyses have established that the out-of-phase relationship between the applied stress and the strain reaction of the polymer causes the heating of the plastic. This loss in energy can be measured and defined for a material as its loss modulus. The transferred energy, on the other hand, is defined via the storage modulus. It may be that if the response of the plastic at the horn contact surface is more in-phase, it is generating less heat. Then, as the ultrasonic wave travels through the polymer, the stress-to-strain relationship becomes more and more out-of-phase due to the interaction with the viscoelastic medium.

Therefore, it is assumed that increasing applied force will improve strength up to the point where solid deformation occurs during welding. For this reason, the maximum force calculation derived above will be used to approximate an ideal force. An improved estimation could be found via finite element analysis. However, it is proposed that this simple equation can provide a rudimentary tool to select a welding force and thus enable a quicker route to initiate process setup for the engineer. As mentioned at the beginning of this section, increased force may negatively affect amorphous polymers' chain orientation.

References

1. Han, C., Lee, K., and Wheeler, N. 1996. Plasticating single-screw extrusion of amorphous polymers: Development of a mathematical model and comparison with experiment. *Polymer Engineering and Science* 36(10).

2. Troughton, M. 2008. *Handbook of Plastics Joining: A Practical Guide*.

3. Palardy, G., Shi, H., Villegas, I., Levy, A., and Le Corre, S. 2018. Experimental investigation of amplitude transmission in ultrasonic welding of thermoplastic composites. *ANTEC*.

4. Baird, D., and Collias, D. 1998. *Polymer Processing*. Hoboken, New Jersey: John Wiley & Sons.

5. Marcus, M. 2018. Methods of polymer weld quality evaluation. *ANTEC*.

6. Grewell, D., Benatar, A., and Park, J., eds. 2003. *Plastics and Composites Welding Handbook*.

7. Gallego-Juarez, J., and Graff, K. 2015. Power ultrasonics: Applications of high-intensity ultrasound.

8. Grewell, D., and Benatar, A. 2008. Semi-empirical, squeeze flow, and intermolecular diffusion model. i. determination of model parameters. *Polymer Engineering and Science*: 860–867.

9. Chuah, Y., Chien, L., Chang, B., and Liu, S. 2000. Effects of the shape of the energy director on far-field ultrasonic welding of thermoplastics. *Polymer Engineering and Science* 40(7): 157–167.

10. Ferry, J. 1980. *Viscoelastic Properties of Polymers*. John Wiley & Sons.

11. Sancaktar, E. 1999. Polymer adhesion by ultrasonic welding. *Journal of Adhesion Science and Technology* 13(2): 179–201.

12. Levy, A., Le Corre, S., and Villegas, F. 2014. Modeling of the heating phenomena in ultrasonic welding of thermoplastic composites with flat energy directors. *Journal of Materials Processing Technology* 214: 1361–1371.

13. Suresh, K., Roopa Rani, M., Prakasan, K., and Rudramoorthy, R. 2007. Modeling of temperature distribution in ultrasonic welding of thermoplastics for various joint designs. *Journal of Materials Processing Technology* 186: 138–146.

14. Marcus, M., Wenning, J., Parsons, J., and Savitski, A. 2016. Comparative analysis of energy director styles on polybutylene terephthalate (PBT) with servo-driven ultrasonic welder. *ANTEC*.

15. Broek, D. 1983. Elementary engineering fracture mechanics.

16. Shenoy, A., Chattopadhyay, S., and Nadkarni, V. 1983. From melt flow index to rheogram. *Rheologica Acta* 22: 90–101.

17. Rawendaal, C. 1988. Polymer extrusion.

18. Shenoy, A., Saini, D., and Nadkarni, V. 1984. Melt rheology of polymer blends from melt flow index. *International Journal of Polymeric Materials* 10(3): 213–235.

19. Grewell, D. 1996. Amplitude and force profiling studies in ultrasonic welding of thermoplastics. *ANTEC*.

20. He, F. 1996. Effect of Amplitude and Pressure Control on the Strength of Ultrasonically Welded Thermoplastics. *ANTEC*.

MIRANDA MARCUS (*mmarcus@ewi.org*) is with the Edison Welding Institute, Columbus, Ohio. **EROL SANCAKTAR** is with the University of Akron, Akron, Ohio .